Dynamics & sparsity in latent threshold factor models: A study in multivariate EEG signal processing

Jouchi Nakajima[a] **and Mike West**[b]

[a]*Bank for International Settlements*
[b]*Duke University*

Abstract. We discuss Bayesian analysis of multivariate time series with dynamic factor models that exploit time-adaptive sparsity in model parametrizations via the latent threshold approach. One central focus is on the transfer responses of multiple interrelated series to underlying, dynamic latent factor processes. Structured priors on model hyper-parameters are key to the efficacy of dynamic latent thresholding, and MCMC-based computation enables model fitting and analysis. A detailed case study of electroencephalographic (EEG) data from experimental psychiatry highlights the use of latent threshold extensions of time-varying vector autoregressive and factor models. This study explores a class of dynamic transfer response factor models, extending prior Bayesian modeling of multiple EEG series and highlighting the practical utility of the latent thresholding concept in multivariate, non-stationary time series analysis.

1 Introduction

In high-dimensional time series analysis, the need to define time-varying patterns of sparsity in model parameters has proven challenging. Dynamic latent thresholding, introduced in Nakajima and West (2013a), provides a general approach that induces parsimony into time series model structures with potential to reduce effective parameter dimension and improve model interpretations as well as forecasting performance. The utility of various classes of latent threshold models (LTMs) has been demonstrated in recent applied studies in macroeconomics (Nakajima and West (2013a), Kimura and Nakajima (2016)) and financial forecasting and portfolio decisions (Nakajima and West (2013b), Zhou, Nakajima and West (2014)). The scope of the approach includes dynamic regressions, dynamic latent factor models, time-varying vector autoregressions, and dynamic graphical models of multivariate stochastic volatility, and also opens a path to new approaches to dynamic network modeling (Nakajima and West (2015)).

This paper adapts the latent thresholding approach to different classes of multivariate factor models with a one main interest in dynamic transfer response analysis. Our detailed case-study concerns time-varying lag/lead relationships among

multiple time series in electroencephalographic (EEG) studies. Here the latent threshold analysis of such models induces relevant, time-varying patterns of sparsity in otherwise time-varying factor loadings matrices, among other model features. We evaluate and compare two different classes of models in the EEG study, and explore a number of posterior summaries in relation to this main interest.

Time series factor modeling has been an area of growth for Bayesian analysis in recent years. Two key themes are: (i) dynamic factor models, where latent factors are time series processes underlying patterns of relationships among multiple time series (e.g., Aguilar et al. (1999), Pitt and Shephard (1999), Aguilar and West (2000), Koop and Potter (2004), Bernanke, Boivin and Eliasz (2005), Lopes and Carvalho (2007), Del Negro and Otrok (2008), Koop and Korobilis (2010)); and (ii) sparse factor models, where the bipartite graphs representing conditional dependencies of observed variables on factors are not completely connected (e.g., West (2003), Lucas et al. (2006), Carvalho et al. (2008), Lucas, Carvalho and West (2009), Yoshida and West (2010), Carvalho, Lopes and Aguilar (2011), Bhattacharya and Dunson (2011)), increasingly applied in problems of classification and prediction.

Here we combine dynamics with sparsity. Some of the practical relevance of models with time-varying factor loadings is evident in recent studies (e.g., Lopes and Carvalho (2007), Del Negro and Otrok (2008), Carvalho, Lopes and Aguilar (2011)). As the number of variables and factors increase, so does the need to induce sparsity in loadings matrices to reflect the view that variables will typically be conditionally dependent on only a subset of factors. In a time series setting, however, the patterns of occurrence of zeros in otherwise time-varying factor loadings matrices may also be time-varying. One factor may relate to one particular variable with a time-varying loading over a period of time, but be insignificant for that variable in other time periods. Thus, the need to develop models of time-varying sparsity of loadings matrices in dynamic factor models.

Conventions and notation

All vectors are column vectors. We use $\boldsymbol{y} \sim N(\boldsymbol{a}, \boldsymbol{A})$, $d \sim U(a, b)$, $p \sim B(a, b)$, $v \sim G(a, b)$, $\boldsymbol{U} \sim W(c, \boldsymbol{D})$, for the normal, uniform, beta, gamma, and Wishart distributions, respectively. Succinct notation for ranges uses $s : t$ to denote $s, s + 1, \ldots, t$ when $s < t$; for example, $\boldsymbol{y}_{1:T}$ denotes $\{\boldsymbol{y}_1, \ldots, \boldsymbol{y}_T\}$. The indicator function is $I(\cdot)$ and diag$(\cdot)$ is the diagonal matrix with diagonal elements in the argument and hence dimension implicit. Elements of any c-vector time series $\boldsymbol{v}_t$ are v_{jt}, $(j = 1 : c)$, and those of any $c \times d$ matrix time series $\boldsymbol{V}_t$ are v_{ijt} $(i = 1 : c, j = 1 : d)$.

2 Dynamic factor models

In a general setting, the m-vector time series $\boldsymbol{y}_t = (y_{1t}, \ldots, y_{mt})'$ $(t = 1, 2, \ldots)$ is modeled as

$$\boldsymbol{y}_t = \boldsymbol{A}_t \boldsymbol{z}_t + \boldsymbol{B}_t \boldsymbol{f}_t + \boldsymbol{v}_t, \qquad \boldsymbol{v}_t \sim N(\boldsymbol{0}, \boldsymbol{\Sigma}_t), \tag{1}$$

where

- $\boldsymbol{z}_t$ is a q-vector of predictor variables known at time t;
- $\boldsymbol{A}_t$ is the $m \times q$ matrix of regression coefficients at time t;
- $\boldsymbol{f}_t$ is the $r \times 1$ vector of latent factors, arising from some underlying latent factor process over time;
- $\boldsymbol{B}_t$ is the $m \times r$ matrix of factor loadings at time t;
- $\boldsymbol{v}_t$ is the residual term, assumed zero-mean normal with diagonal variance matrix $\boldsymbol{\Sigma}_t = \mathrm{diag}(\sigma_{1:m,t}^2)$ of volatilities σ_{jt} at time t.

Complete specification requires models for $\boldsymbol{f}_t$, $\boldsymbol{A}_t$, $\boldsymbol{B}_t$ and σ_{jt} over time. Typically, $m \gg r$, and models are identified via constraints on $\boldsymbol{B}_t$, such as fixing $\boldsymbol{B}_t$ to have zeros above a unit upper diagonal: $b_{iit} = 1$ and $b_{ikt} = 0$ for $i = 1 : r, k = i + 1 : r$. In Section 3, there is interpretable structure to $\boldsymbol{f}_t$ and alternative assumptions are natural. Special cases and assumptions now follow.

Constant and sparse factor models

Much past work uses constant coefficients $\boldsymbol{A}_t = \boldsymbol{A}$ and loadings $\boldsymbol{B}_t = \boldsymbol{B}$. The pure factor model, with $\boldsymbol{A}_t \boldsymbol{z}_t = \boldsymbol{0}$ and $\boldsymbol{B}_t = \boldsymbol{B}$, typically assumes the factors $\boldsymbol{f}_t$ are zero-mean and independent, yielding a linear factor representation of the conditional variance matrix of $\boldsymbol{y}_t$. Sparsity in $\boldsymbol{B}$ then begins development of more parsimonious models for larger m, r (e.g., West (2003)).

FAVAR models

When $\boldsymbol{z}_t$ concatenates past values $\boldsymbol{y}_{t-j}$ $(j = 1 : d)$ to lag d, and $\boldsymbol{A}_t = \boldsymbol{A}$, $\boldsymbol{B}_t = \boldsymbol{B}$ are constant, the model is a factor-augmented vector autoregression (FAVAR). Variants based on differing models for $\boldsymbol{f}_t$ are becoming of increasing interest in macroeconomics (Bernanke, Boivin and Eliasz (2005), Koop and Korobilis (2010)).

Factor stochastic volatility models

Traditional Bayesian multivariate volatility models have $\boldsymbol{A}_t = \boldsymbol{0}$, $\boldsymbol{B}_t = \boldsymbol{B}$, and $\boldsymbol{f}_t \sim N(\boldsymbol{0}, \boldsymbol{\Gamma}_t)$ where $\boldsymbol{\Gamma}_t = \mathrm{diag}(\gamma_{1:r,t}^2)$. Model completion involves stochastic volatility model for the γ_{jt} and σ_{jt}, based on either log-AR(1) models or Bayesian discounting (e.g., Aguilar et al. (1999), Pitt and Shephard (1999), Aguilar and West (2000), Prado and West (2010)).

Time-varying regression and factor loadings models

Variants of models with time-varying A_t, B_t are well-used (e.g., West and Harrison (1997), Prado and West (2010), West (2013)). Typically, the elements a_{ijt}, b_{ijt} are AR(1) processes. Within this class, random walk models have flexibility to adapt to change over time, while stationary AR(1) models can have longer-term predictive value and interpretation (Lopes and Carvalho (2007), Del Negro and Otrok (2008), Nakajima and West (2013a, 2013b)).

Process models for factors

Models of factor processes f_t typically involve either conditionally independent factors over time, with or without time-varying conditional variances, or stationary vector autoregressive (VAR) models.

3 Dynamic factor models and transfer responses

3.1 Introductory comments

We highlight example models that incorporate elements noted in Section 2, while being customized to the EEG study: a response variable is hierarchically linked to current and lagged values of an underlying latent process of scientific interest. A first latent factor model is discussed, then extended with a time-varying vector autoregressive component; these two models are customized examples of time-varying FAVAR processes.

3.2 Model M: A dynamic transfer response factor model

A dynamic transfer response factor model (DTRFM) relates the outcome variables to a foundational, scalar latent process x_t by specifying f_t to be a vector of recent values of this underlying scalar process. Each outcome variable relates to potentially several recent and lagged values of x_t through time-varying loadings coefficients; at any instant in time, these coefficients define the transfer response of the variable to the history of the underlying process. As the loadings vary in time, the form of this response then naturally varies. The basic structure of the model is described here.

   In equation (1), set $A_t z_t = 0$ for all t. Suppose also that

$$f_t = (x_t, x_{t-1}, \ldots, x_{t-r+1})',$$

for some $r > 0$, where the scalar series x_t is modeled as a time-varying autoregressive (TVAR) process of order p. That is,

$$x_t = \sum_{j=1:p} \delta_{jt} x_{t-j} + \varepsilon_t, \qquad \varepsilon_t \sim N(0, w_t), \tag{2}$$

$$\delta_t = \delta_{t-1} + \xi_t, \qquad \xi_t \sim N(\mathbf{0}, \mathbf{\Psi}), \tag{3}$$

where $\boldsymbol{\delta}_t = (\delta_{1t}, \ldots, \delta_{pt})'$ is the vector of AR coefficients at time t. Conditional on the variance elements $w_{1:T}$ and $\boldsymbol{\Psi}$, the stochastic sequences $\boldsymbol{\nu}_t$ (of equation (1)), ε_t and $\boldsymbol{\xi}_t$ are assumedly independent over time and mutually independent. Equation (3) indicates that the $\boldsymbol{\delta}_t$ coefficients follow a vector random walk over time, permitting time variation but not anticipating its direction or form. Coupled with equation (2) we have the traditional specification of a Bayesian TVAR(p) model for the latent x_t process.

For the ith scalar response variable, the above model implies

$$y_{it} = \sum_{k=0:r-1} b_{ikt}x_{t-k} + v_{it}, \qquad v_{it} \sim N(0, \sigma_{it}^2), \tag{4}$$

showing the transfer of responses from past values of x_t via the—possibly quite widely time-varying—loadings b_{ikt}, the latter specific to series i, for each $i = 1 : m$.

Model identification is straightforward. From equation (4), it is clear that an identification problem exists with respect to the lag/lead structure, that is, the time origin for the latent x_t process, as well as the scale of x_t relative to the b_{ikt}. Fixing elements of one row of $\boldsymbol{B}_t$ to specified values obviates this. Here we do this on the first row: for one factor (lag) index $s \in \{1 : r\}$, we set $b_{1st} = 1$ and $b_{1kt} = 0$ for $k = 1 : r, k \neq s$. This way, y_{1t} is a direct, unbiased measurement of x_{t-s+1}, subject to residual noise, so that we have formal identification and a quantitative anchor for prior specification.

Beyond the need for priors for model hyper-parameters, we need structures for the error volatility processes σ_{it} in equations (1), (4) and the TVAR innovations variance process w_t in equation (2). For routine analysis that is not inherently focused on volatility prediction, standard Bayesian variance discount learning models—effective random walks whose variability is controlled by a single discount factor—are defaults. Specified to describe typically slowly, randomly changing variances, the inverse gamma/beta Bayesian model has the ability to track time-varying variances over time, and to deliver full posterior samples from relevant conditional posteriors for volatility sequences in MCMC analyses. We use variance discount models here, based on standard theory in, for example, Chapter 10 of West and Harrison (1997) and Chapter 4 of Prado and West (2010); these are simply specified via two discount factor hyper-parameters: λ_σ, for each of the set of observation volatilities, and λ_w for the TVAR innovations volatility.

3.3 Latent components and dynamic transfer responses

Substantive interpretation is aided by investigating the more detailed structure that theoretically underlies the latent TVAR process x_t. Specifically, well-known (and well-exploited) time series decomposition theory (e.g., West (1997, 2013), West and Harrison (1997), Prado and West (2010)) shows that, given the model parameters, the x_t series has the decomposition

$$x_t = \sum_{g=1:\tilde{p}_t} \tilde{x}_{gt} + \sum_{h=1:\hat{p}_t} \hat{x}_{ht}, \tag{5}$$

where the $\tilde{x}_{gt}, \hat{x}_{ht}$ are "simpler" component time series processes and $\tilde{p}_t, \hat{p}_t$ are non-negative integers such that $2\tilde{p}_t + \hat{p}_t = p$. The values of these integers and the nature of the component processes depend on the model parameters $\boldsymbol{\delta}_t$. Typically, slow variation over time in these yields stable numbers $\tilde{p}_t, \hat{p}_t$ and the resulting processes are computable directly from (posterior samples or estimates of) the x_t and $\boldsymbol{\delta}_t$. The component processes $\tilde{x}_{gt}$ have the (approximate) forms of time-varying autoregressive moving averages—TVARMA(2, 1) processes—exhibiting quasi-periodic behavior: each $\tilde{x}_{gt}$ is a stochastic sine wave whose amplitude, phase and frequency varies in time; the time variation in frequency is directly related to that in $\boldsymbol{\delta}_t$, while the amplitude and phase variation is inherent and driven by the levels of variation controlled by w_t. Further, posterior inferences for the time-varying frequencies, amplitude and phase are directly available from posterior simulations that generate samples of the x_t and $\boldsymbol{\delta}_t$ at each time. In parallel, each $\hat{x}_{ht}$ is a TVAR(1) process, with time variation in short-term autocorrelations driven by that in $\boldsymbol{\delta}_t$. As with the $\tilde{x}_{jt}$, we have direct access to posterior inferences on the TVAR(1) parameters of these component processes from simulations of the posterior for $x_t, \boldsymbol{\delta}_t$ at each time. This decomposition therefore gives inferences on underlying time-frequency and short-term dependency structures underlying x_t and its dynamic behavior.

From equations (4), (5), it follows that

$$y_{it} = \sum_{g=1:\tilde{p}_t} \tilde{y}_{igt} + \sum_{h=1:\hat{p}_t} \hat{y}_{iht} + v_{it},$$

where, for each g, h in the ranges displayed,

$$\tilde{y}_{igt} = \sum_{k=1:r-1} \beta_{ikt}\tilde{x}_{gt} \quad \text{and} \quad \tilde{y}_{iht} = \sum_{k=1:r-1} \beta_{ikt}\tilde{x}_{ht}.$$

Thus the transfer response pattern defined by the time-varying factor loadings translates the nature of the inherent, underlying components of the "driving" x_t process to each of the output/response variables.

The above shows that this class of models provides broad scope for capturing multiple time-varying patterns of component structure—including several or many components with dynamically varying time-frequency characteristics—via a single latent process filtered to construct the latent factor vector process $\boldsymbol{f}_t$ in the general framework. The flexibility of these models for increasingly high-dimensional response series $\boldsymbol{y}_t$ is then further enhanced through the ability of models with series-specific and time-varying loadings b_{ikt} to differentiate both instantaneous and time-varying patterns in the transfer responses.

3.4 Model M+: DTRFM with a time-varying VAR component

A direct model extension adds back a non-zero dynamic regression term to provide an example of time-varying FAVAR models. That is, with the dynamic factor

component as specified via Model M, suppose $\boldsymbol{y}_t$ now follows equation (1) where $q = m$, the $m \times m$ matrix $\boldsymbol{A}_t$ contains time-varying autoregressive parameters and $\boldsymbol{z}_t = \boldsymbol{y}_{t-1}$. That is, $\boldsymbol{y}_t$ is dynamically regressed on the immediate past value $\boldsymbol{y}_{t-1}$ as well as the underlying components of a driving latent process through the dynamic transfer response mechanism: we denote this as a TV-VAR(1) component of the model.

This extension of Model M allows for the transfer response effects of the fundamental, driving x_t process to be overlaid with spill-over effects between individual response series from one time point to the next, modeled by a basic TV-VAR(1) component. This can be regarded as a model extension to assess whether the empirical TV-VAR component is able to explain structure in the response data not adequately captured by the structure dynamic factor component. For increasingly large m, the TV-VAR(1) model component alone (i.e., setting $\boldsymbol{B}_t = \boldsymbol{0}$), implies what can be quite flexible marginal processes for the individual y_{it}; in contrast, the dynamic transfer response factor component—while also quite flexible—represents structurally related processes. There is thus opportunity to for evaluation of the latter in the extended Model M+.

4 Dynamic sparsity and latent thresholding

4.1 Thresholding of dynamic parameter processes

As the dimension m of response variables and the number r of effective latent factors increases, it becomes increasingly untenable to entertain models in which all loadings in $\boldsymbol{B}_t$ are non-zero. Further, depending on context, it is also scientifically reasonable to entertain models in which one or more variables may relate—in a time-varying manner—to a particular element of the latent factor vector for some periods of time, but that the relationships may be practically negligible at other epochs. This is the concept of dynamic sparsity: a particular b_{ikt} may be non-zero over multiple, disjoint time periods, and adequately modeled by a specified stochastic process model when non-zero, but effectively zero in terms of the effect of f_{kt} on y_{it}, in other periods. The same idea applies to dynamic regression and/or autoregressive parameters in $\boldsymbol{A}_t$. Analysis that permits this will allow for adaptation over time to zero/non-zero periods as well as to inference on actual values when non-zero. This includes extreme cases when a b_{ikt} may be inferred as effectively zero (or non-zero) over the full time period of interest.

Dynamic latent thresholding (Nakajima and West (2013a, 2013b)) addresses this question of *time-varying sparsity* in some generality; this approach is now developed in our context of dynamic transfer response factor models. We anchor the development on basic AR(1) process models for the free elements of the dynamic factor loadings matrix $\boldsymbol{B}_t$, recalling that the first row of elements is constrained

to fixed (0/1) values as noted in Section 3.2. For $i = 2 : m, k = 1 : r$, the b_{ikt} are modeled via what we denote by the LT-AR(1) processes defined as follows:

$$b_{ikt} = \beta_{ikt} s_{ikt} \qquad \text{with } s_{ikt} = I(|\beta_{ikt}| \geq d_{ik}), \tag{6}$$

where the latent process β_{ikt} is AR(1) with

$$\beta_{ikt} = \mu_{ik} + \phi_{ik}(\beta_{ik,t-1} - \mu_{ik}) + \eta_{ikt}, \qquad \eta_{ikt} \sim N(0, v_{ik}^2), \tag{7}$$

and where $|\phi_{ik}| < 1$. The processes are assumed independent over i, k. The latent threshold structure allows each time-varying factor loading to be shrunk fully to zero when its absolute value falls below a threshold d_{ik}. This way, a factor loads in explaining a response only when the corresponding β_{ikt} is "large enough". Inference on the latent β_{ikt} processes and threshold parameters make this data-adaptive, neatly embodying and yielding data-informed time-varying sparsity/shrinkage and parameter reduction.

The same approach applies to the time-varying autoregressive parameters in the extension to Model M+. That is, the effective model parameters $A_t = (a_{ijt})_{i,j=1:m}$ are modeled as thresholded values of AR(1) processes α_{ijt} in precisely the same way as for the b_{ikt}. Details are left to the reader as they follow the development for B_t with simple notational changes.

4.2 Structured priors on thresholds

It will be evident that prior specification for threshold parameters d_{ik} are key in defining practical models. We can do this by referencing the expected range of variation of the corresponding β_{ikt} process. Under the AR(1) process model detailed above, β_{ikt} has a stationary normal distribution with mean μ_{ik} and variance $u_{ik}^2 = v_{ik}^2/(1 - \phi_{ik}^2)$. Given the hyper-parameters $(\mu_{ik}, \phi_{ik}, v_{ik})$, this allows us to compute the probability that β_{ikt} exceeds the threshold—i.e., the probability of a practically significant coefficient—across any range of possible thresholds. Nakajima and West (2013a) follow this logic to specify informative, structured priors for d_{ik} that depend explicitly on $(\mu_{ik}, \phi_{ik}, v_{ik})$. We use this specification here; in particular, take conditional uniform priors

$$d_{ik}|K, \mu_{ik}, \phi_{ik}, v_{ik} \sim U(0, |\mu_{ik}| + Ku_i),$$

for some $K > 0$. Direct evaluation then yields marginal (with respect to d_{ik}) sparsity probabilities

$$\Pr(s_{ikt} = 1|K) \equiv \Pr(|\beta_{ikt}| > d_{ik}|K)$$
$$= 2 - 2\Phi(K) - 2K^{-1}\phi(K) + K^{-1}2^{1/2}\pi^{-1/2},$$

where $\Phi(\cdot)$ is the standard normal c.d.f. This is trivially evaluated. For large K, this is also very well approximated by $K^{-1}2^{1/2}\pi^{-1/2}$ (this is extremely accurate for K as low as 2 and practically relevant values of K exceeding that). The sparsity probability strictly decreases in K and decays to values of about 0.25, 0.20

and 0.15, respectively, at about $K = 3.2, 4$ and 5.3, respectively. This gives us assessment of what a particular choice of K implies in terms of overall expected levels of sparsity *a priori*. We find strong robustness in posterior inferences to specified values of K above 3 or so, and use that value as a default. Note also that there is flexibility to customize the prior to use different K values for each threshold, to cater for contexts in which we aim to favor higher thresholds (and hence higher probabilities of zero parameter process values) for some i, k than for others.

4.3 MCMC-based computation

MCMC computations extend those developed for time-varying autoregressions and multivariate stochastic volatility factor models in Nakajima and West (2013a, 2013b). The overall MCMC integrates a series of steps that use standard simulation components from Bayesian state space models (e.g., West and Harrison (1997), Prado and West (2010)) and from traditional (static loadings) latent factor models (Aguilar and West (2000), Lopes and West (2004)). Customization here involves modifications to resample the latent TVAR factor process in our dynamic transfer responses factor context, and to include Metropolis Hastings steps as in Nakajima and West (2013a) for latent threshold components. The Appendix accompanying this paper describes key details, and notes how the MCMC directly extends previously described strategies for dynamic latent threshold models.

## 5 Application: EEG time series analysis

5.1 Background, data and prior modeling approaches

Electroencephalographic (EEG) traces are time series of electrical potential fluctuations at various scalp locations of a human subject, reflecting the complex dynamics of underlying neural communication. Analysis of multichannel EEG traces is key to understanding the impact of electroconvulsive therapy (ECT), one of the most effective treatments known for major depression with electrically induced seizures in patients (Weiner and Krystal (1994)). The convulsive seizure activity drives multichannel EEG traces and statistical interest is to model such multivariate time series in order to reveal underlying characteristics and effects of ECT. Various models have been studied to explore features of EEG time series (e.g., Kitagawa and Gersch (1996), West, Prado and Krystal (1999), Prado, West and Krystal (2001), Prado (2010a, 2010b), Prado and West (2010)). Univariate TVAR forms are proven as models of individual EEG channels (e.g., West, Prado and Krystal (1999), Prado, West and Krystal (2001)); they can adequately represent what can be considerable changes in the patterns of evolution of time-frequency structure in series, as well as differences and changes in relationships across the

EEG channels. Such studies highlight the need for multivariate models of the time-varying commonalities across channels, with latent process structure reflecting the inherent, underlying mechanisms of neural communication.

Our analysis adapts the earlier approach of Prado, West and Krystal (2001). That work was the first Bayesian approach to multivariate time series analysis that incorporated the key scientific feature of a single, focal latent process "driving" the EEG signals across multiple channels. The authors used a novel dynamic distributed lag approach that captures time-varying lag-lead structures across series, introducing a customized model specific to that context. Though effective, that approach was very specific and empirical—the authors developed dynamic regressions of $m - 1$ of the channels on the *observed signal* of one selected channel, the latter chosen as an proxy for the underlying latent driving process x_t. The developments of the current paper provide a general, flexible and—in terms of the specific goals of the dynamic lag/lead study—almost perfectly suited context that can be seen, in part, as an outgrowth from that prior work. Here the identification of dynamically adaptive lag/lead structure is driven by combining time variation in non-zero factor loadings with the latent threshold approach.

The study here explores $m = 19$-channel EEG times series recorded in one seizure of one patient, as reported and earlier analyzed in West, Prado and Krystal (1999) and Prado, West and Krystal (2001). The EEG channels are $m = 19$ electrodes located around and over the patient's scalp; see Figure 1. The original data set has sampling rate 256 Hz over a period of 1–2 minutes; following and to compare directly with Prado, West and Krystal (2001), we analyze the series subsampled every sixth observation after removing about 2000 observations from the beginning (up to a higher amplitude portion of the seizure) yielding $T = 3000$ observations. Representative graphs of data on two of the channels over selected epochs appear in Figure 2. Visual inspection of the substantial time-varying, quasi-periodic trajectories of the data indicates that signals on some EEG channels are
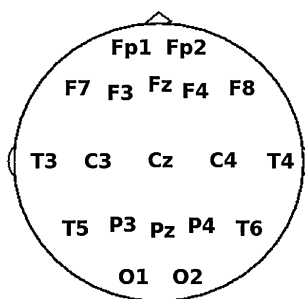
Figure 1 *Representation of the* 19-*electrodes placement over the scalp. The m = 19 series are measurements of electrical potential fluctuations taken in parallel at each of these locations, defining the EEG channels (International* 10–20 *EEG System).*

obviously "delayed" with respect to other channels, and the apparent delays (lags) vary substantially through time. This is perfectly consistent with the dynamic patterns of relationships of individual channels (the y_{it}) with an underlying seizure process (the latent x_t) captured by our model structure (Section 3.3); the latent x_t process represents a range of dynamic quasi-periodicities characterizing multiple brain wave components overlaid by, and modified by, the induced seizure, and the time-varying lag/lead relationships among channels are represented by channel-
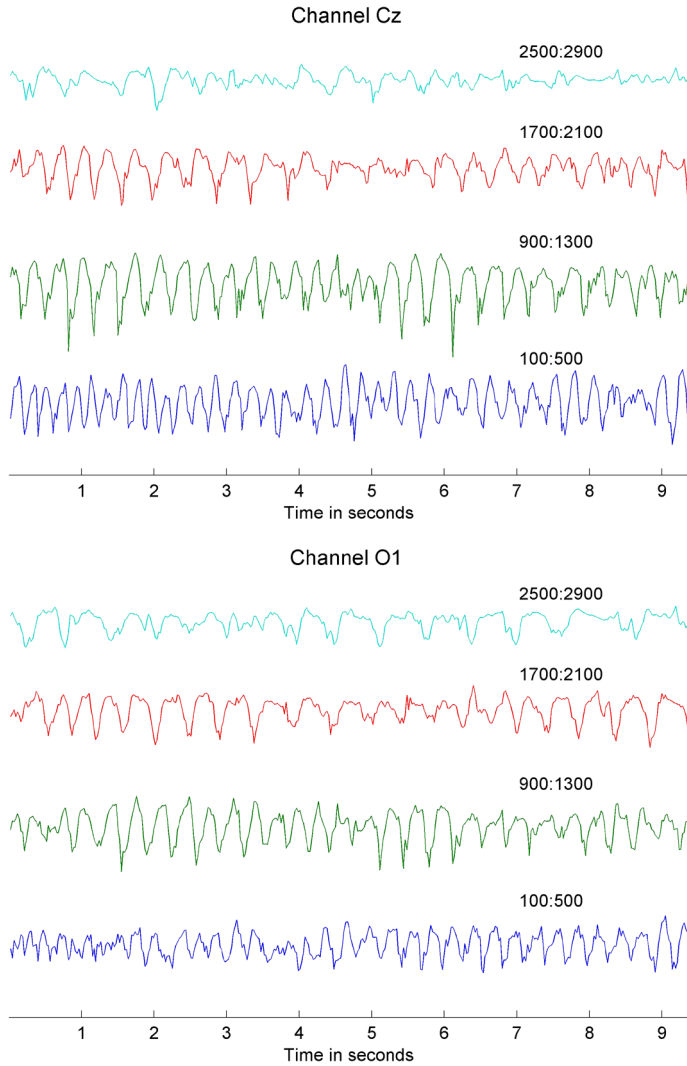
Figure 2 *Sections of time series on two selected EEG channels, with standardization so that the vertical scales of variation in EEG electrical potential are comparable across epochs and channels.*

specific and time-varying factor loadings, some of which may be negligible for all time or for periods of time, and relevant elsewhere.

5.2 DTRFM Model M for multivariate EEG signals

Our analysis summaries are based on $r = 5$ effective lags, i.e., the model has a 5-dimensional latent factor vector $\boldsymbol{f}'_t = (x_t, x_{t-1}, \ldots, x_{t-4})'$ and the first row of $\boldsymbol{B}_t$ set to $(0, 0, 1, 0, 0)$ as the basis for model identification. This precisely parallels the setup in the empirical model of Prado, West and Krystal (2001). As discussed in Section 3.2, some constraints of this form are needed on elements of $\boldsymbol{B}_t$ to formally identify the single latent factor process model. There is no loss of generality nor any superfluous structure imposed on the model here; we could choose any element of the first row of $\boldsymbol{B}_t$ to insert the 1, with different choices simply shifting the implied time origin of the x_t process. Under this structure, the first EEG channel y_{1t} loads only x_{t-2}, while the other channels have loadings in the first (last) two columns of $\boldsymbol{B}_t$ related to the leading (lagged) values of the x_t process.

Our analysis takes the so-called vertex channel Cz as series $i = 1$. See Figure 1. This parallels the use of the observed data on this specific channel as an empirical factor process in Prado, West and Krystal (2001). The other channels are ordered from the centre out. One further modeling detail relates to a modification for a further, subtler "soft" identification question. The model so far implies that $y_{1t} = x_{t-2} + \nu_{1t}$, so the conditional variation expected in channel 1 is the sum of time-varying contributions from the x_t process plus σ_{1t}^2. As in all state-space models with multiple components contributing to variability in observed data, distinguishing and partitioning the contributions requires care in prior specification; the picture is complicated here as time variation in σ_{1t}^2 "competes" with the intricate dynamics of the $\boldsymbol{\delta}_t$ and time variation in w_t. A specification that controls this more usefully in the current latent factor models is to fix as constant the measurement error in series 1, that is, set $\sigma_{1t} = \sigma_1$, constant over time. This ensures the interpretation of ν_{1t} as pure measurement error (there being no reason to expect time variation in pure measurement error variances, as opposed to the characteristics of the underlying factor processes and transfer response/loadings parameters). We do this, maintaining the stochastic variance discount model for the other σ_{jt} ($j = 2 : m$); the latter combine pure measurement error and any other identified changes in residual volatility across these channels. Then, posterior inferences indicating substantial patterns of time variation in the latter then indicate the ability of the discount models to account for relative variability not captured by the underlying, identified latent factor process. The MCMC analysis of Section 4.3 is trivially modified; a traditional inverse gamma prior on σ_1^2 leads to an inverse gamma complete conditional posterior.

The analyses summarized are based on model order $p = 6$ for the latent x_t process. While formal order selection approaches could be entertained (e.g., Huerta and West (1999), Prado and Huerta (2002)), our philosophy based on applied work

with TVAR and related models in many areas is to fit successively larger models and assess practical relevant of resulting inferences. Here we fit the DTRFM with model orders up to $p = 12$, and for each analysis examine the posterior estimates of components $\tilde{x}_{jt}, \hat{x}_{jt}$ as detailed in Section 3.3. With successively higher values of model order p, we find robust estimation of $\tilde{p}_t = 3$ quasi-periodic components with estimated frequencies varying over time in ranges consistent with known ranges of seizure and normal brain wave activity. Model order $p = 6$ is needed to identify these three components, and they persist in models of higher order; in addition to their substantive relevant, the estimated components are sustained over time and vary at practically relevant levels in terms of their contributions to each of the EEG series. However, moving beyond $p = 6$ leads to increasing numbers of estimated components that are very ephemeral, of low amplitudes and higher inferred frequencies beyond the range of substantive relevance. This signals over-fitting as the model caters to finer aspects of what is really noise in the data. Disregarding such estimated noise components is certainly acceptable, and so we prefer to cut-back to the model order $p = 6$ that identifies the main component structures without these practically "spurious" elements.

Model specification is completed with priors for hyper-parameters. We take $\sigma_1^{-2} \sim G(500, 10^4)$, supporting a range of values for σ_1 and with prior mean for σ_1 near 4.5. Seizure EEG data typically range over 300–600 units on the potential scale, with sample standard deviations over selected epochs varying from 40–100 or more. Hence, an expectation of measurement error standard deviation around 4–5 is consistent with prior expectations that measurement error constitutes in the range of 4–12% of the signal uncertainty in the traces. For the stochastic discount variance models, we set values of the discount factors as $\lambda_w = \lambda_\sigma = 0.99$; this is based in part on examination of analyses with various values, and consistent with relatively modest levels of volatility in variance components. Priors for the hyper-parameters of the latent AR(1) parameter processes are as follows: $1/v_{ik}^2 \sim G(50, 0.01)$, $(\phi_{ik} + 1)/2 \sim B(20, 1.5)$, and $\mu_{ik} \sim N(0, 1)$, independently, for $i = 2 : m, k = 1 : r$. This anticipates persistence in non-thresholded latent factor loadings, while allowing for some of the loadings to exhibit notable patterns of change. Finally, we take $\mathbf{\Psi}^{-1} \sim W(100, 10^{-3}I)$ and set $K = 3$ in the conditional uniform priors for thresholds.

5.3 Some posterior summaries from analysis of DTRFM Model M

Summaries here come from $J = 20,000$ MCMC draws after a burn-in period of 5000. Computations were performed using custom code in Ox (Doornik (2006)).

Figure 3 displays time trajectories of the posterior means of the factor process x_t, and the volatility $w_t^{1/2}$ of its driving innovations. The figure displays similar trajectories for the time-varying characteristic frequency and modulus for each of the three identified quasi-periodic components in x_t, the $\tilde{x}_{jt}$ of Section 3.3. The $\tilde{x}_{jt}$ component of lowest frequency has oscillations in the so-called "seizure" or "slow
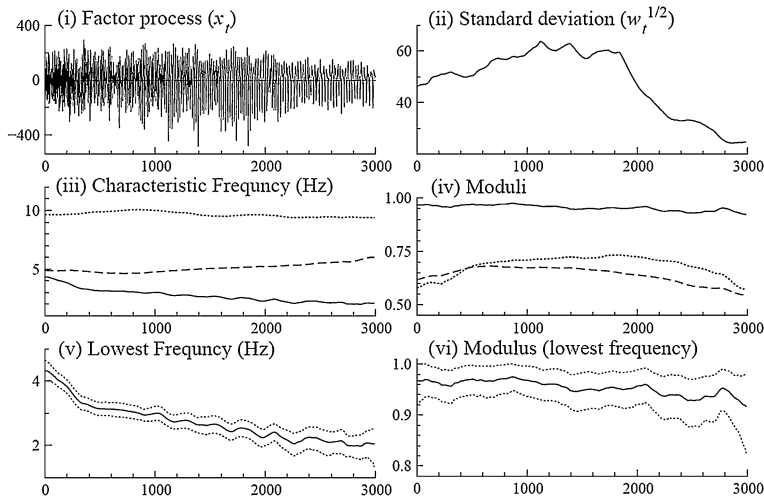
Figure 3 *Elements of inference on the latent factor process and its components in the EEG analysis. The trajectories are posterior means of: (i) the factor process x_t, and (ii) the innovation volatility process $w_t^{1/2}$; (iii) the characteristic frequencies, and (iv) moduli of the three quasi-periodic components $\tilde{x}_{jt}$, $j = 1:3$; and (v) the characteristic frequency, and (vi) modulus of the lowest-frequency component (solid) with 95% credible intervals (dotted).*

wave" band, considerably decaying toward the end of the seizure episode. Notably, the other two inferred components have characteristic frequencies and moduli that are rather stable over time though exhibit minor variation.

The frequency trajectories of the three quasi-periodic components show that each lies in one of the expected neuropsychiatric categories: the so-called *delta* band (roughly 0–4 Hz), *theta* band (4–8 Hz), and *alpha* band (8–13 Hz) (Dyro (1989)). Each component process $\tilde{x}_{jt}$ is defined by the corresponding characteristic frequency, while being broad-band in the spectral domain with time-varying spectra that can be understood to peak at the characteristic frequencies themselves. The lowest-frequency component stays in the *delta* range and gradually decreases over time; its modulus is close to one (solid line in Figure 3(iv)), which indicates a considerably persistent component; this so-called delta-slow wave dominates the factor process during the course of the seizure, while its frequency content slides towards lower values towards the end of the seizure episode. The other two quasi-periodic components lie in the *theta* and *alpha* ranges; their moduli and amplitudes are lower than those of the dominant component over the whole seizure course, and show only limited changes over time. These reflect known frequency ranges of normal brain signaling, being dominated through much of the period by the strong seizure waveform. The innovations volatility rises in the initial part of the seizure to drive increased amplitude fluctuations throughout the central section, and then decays in later stages corresponding to the control and dissipation of the
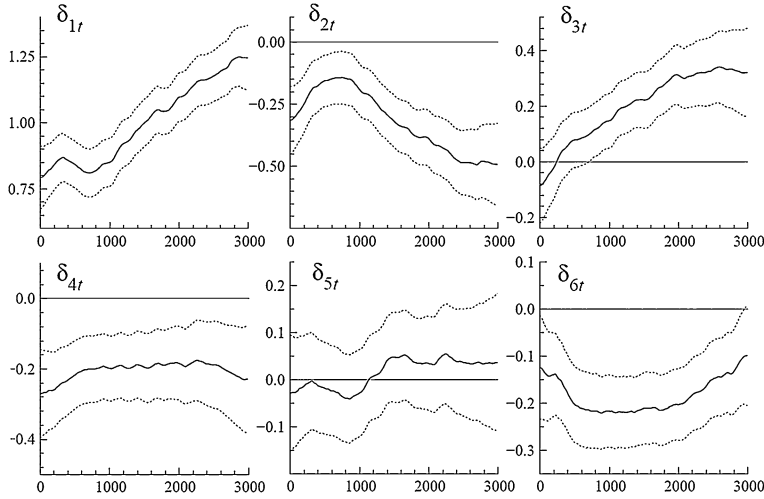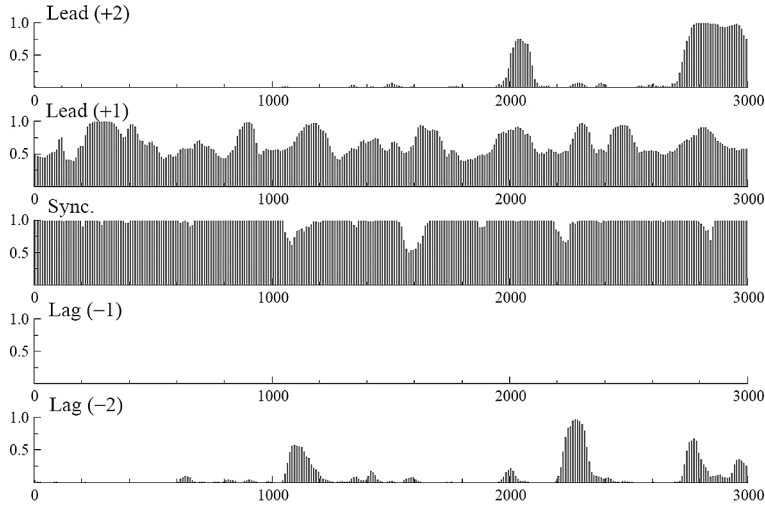
Figure 4 *EEG analysis*: *Trajectories of posterior means* (*solid*) *and* 95% *credible intervals* (*dotted*) *for the TVAR coefficients* $\delta_{1:6,t}$.

brain seizure effects. These features are consistent with expected structure in the seizure process, and with the broad results of Prado, West and Krystal (2001).

Figure 4 provides the trajectories of the posterior means and 95% credible intervals for the TVAR coefficients $\delta_{1:p,t}$. All are markedly time-varying. The 95% credible intervals are slightly wider during the late time periods, which feeds through to increased uncertainties in features of the quasi-periodic components; Figures 3(v) and (vi), displaying the posterior means and 95% credible intervals of the frequency and modulus for the lowest-frequency component respectively, showing somewhat increased uncertainties towards the end of the seizure.

To generate some insights into the nature of dynamic sparsity under the latent threshold model, we select one channel—F7 at $i = 4$,—and plot the corresponding trajectories of the estimated posterior probabilities $\Pr(s_{ikt} = 1 | \mathbf{y}_{1:T})$ over time; i.e., the probability of a non-zero loading of channel F7 on each of the values x_{t-k} for $k = 0 : r - 1$. See Figure 5 where we indicate the loadings on x_t, x_{t-1} by Lead($+2$) and ($+1$) respectively, that on x_{t-2} by Sync, and those on x_{t-3}, x_{t-4} by Lag(-1) and (-2) respectively. The annotation here refers to lead/lag relative to the vertex location Cz that reads-out an unbiased estimate of x_{t-2}. So a non-zero loading of F7 on x_t, for example, defines a 2-period lead of that channel relative to the vertex, whereas a non-zero loading on x_{t-3} represents a 1-period lag relative to the vertex channel Cz, and so forth. From the figure, it is clearly inferred that there is strong synchrony between F7 and Cz in their transfer responses to fluctuations in x_t based on the Sync trajectory. Also, F7 also has a reasonable probability of responding to the latent factor process x_t 1-period ahead of Cz, and almost surely does not lag Cz in the transfer response over most of the time period, nor lead by more than 1 period until perhaps later in the seizure episode. The ability of latent thresholding

Figure 5 *EEG analysis*: *Trajectories of posterior probabilities* $\Pr(s_{ikt} = 1 | \boldsymbol{y}_{1:T})$ *for channel F7, index* $i = 4$, *indicating the inferred probabilities of lag-lead structure in transfer response to* x_t *as they vary over time.*

to adaptively indicate existence of non-zero loadings during some periods and not others, while also operating as a "global" variable selection mechanism as well, is nicely exemplified here.

Figure 6 provides a visual display of posterior probabilities $\Pr(s_{ikt} = 1 | \boldsymbol{y}_{1:T})$ across all the channels $i = 1 : 19$, and drawn at selected snapshots in time, with images created by linearly interpolating between the estimates at the electrode locations. Note that the model says nothing about spatial relationships between channels. The marked patterns of shrinkage in the latent threshold model analysis does nevertheless indicate strong spatial relationships, while the relationships also show marked patterns of change over time. For example, loadings of Lead(+2) are commonly and globally shrunk to zero from left frontal to right occipital sites. The Lead(+2) loadings around right frontal and prefrontal areas exhibit evolving degree of shrinkage. Similar changes are found in the parietal and occipital regions of Lag(−2) loadings. Meanwhile, almost no shrinkage is found in the synchronized loadings except for the channel T3 (left temporal).

Figure 7 is a companion to Figure 6 that exhibits aspects of estimated factor loadings with the lag-lead structure at selected time points. The images represent estimates $\hat{b}_{ikt} = E(\beta_{ikt} | \boldsymbol{y}_{1:T}) \hat{s}_{ikt}$ where $\hat{s}_{ikt} = 1$ if $\Pr(s_{ikt} = 1 | \boldsymbol{y}_{1:T}) > 0.5$ and zero otherwise. Recall that the factor loading of vertex channel Cz is fixed at 1 for the basis and 0 for lagged/leaded times. The estimates show strong patterns of positive spatial dependencies with Cz at the synchronized state (zero lag/lead), with concurrent loadings on the x_t process decaying towards the exterior regions. The approximate centroid of the higher loadings region moves from front to back
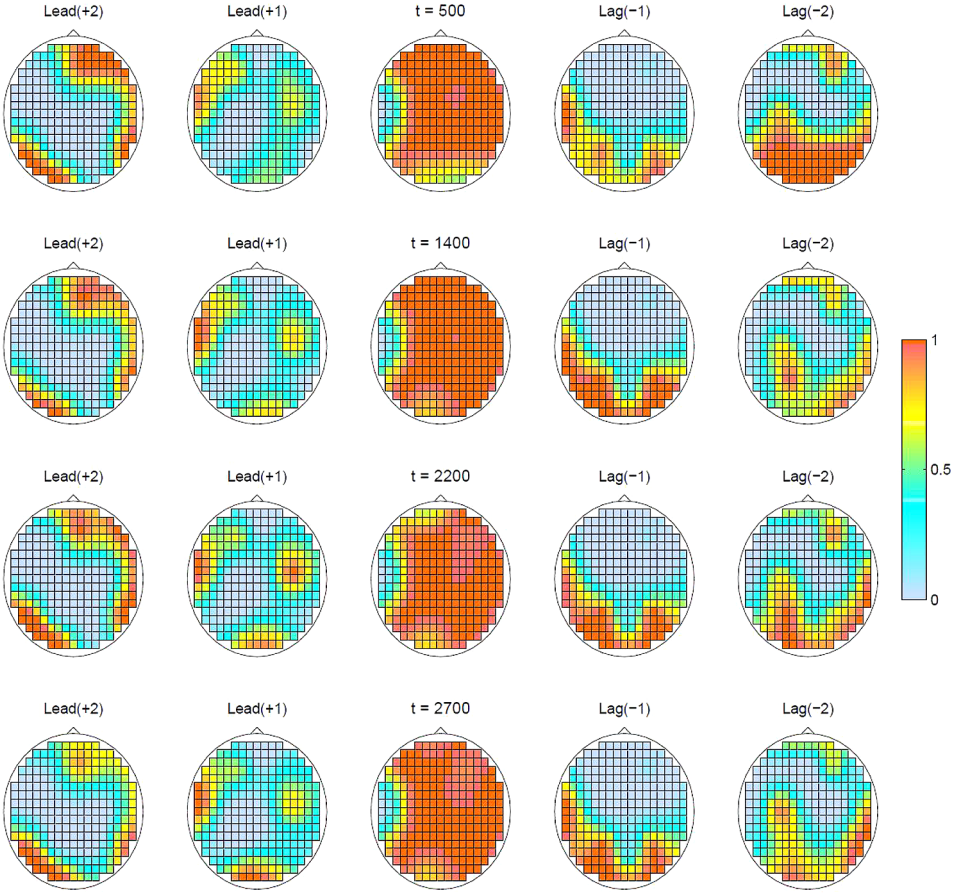
Figure 6 *EEG analysis: Contoured values of* $\Pr(s_{ikt} = 1|\mathbf{y}_{1:T})$ *interpolating from values at the channels* $i = 1:19$. *Each row corresponds to the values at a selected time point, and the columns represent the indices* k *in relation to the transfer responses to* x_{t-k} *for* $k = 0 : r - 1$.

through the course of the seizure, consistent with what is understood to be the typical progression of seizure waveforms (Prado, West and Krystal (2001)). In the third row of the figure ($t = 2200$), the highest loadings appears at and near channel Pz, and the parietal region exhibits rising intensity. Another higher intensity is detected around the right temporal area in Lead($+2$) and in the channel C4 in Lead($+1$). This indicates dynamics of the driving latent process exhibited earlier in right temporal/central areas and followed in the occipital region; this spatial asymmetry in estimated transfer response loadings again links to experimental expectations for the progression of seizure activity. In the last row of the figure ($t = 2700$, a late stage of the seizure), the major lead/lag loadings diminish while the synchronized loadings persist.
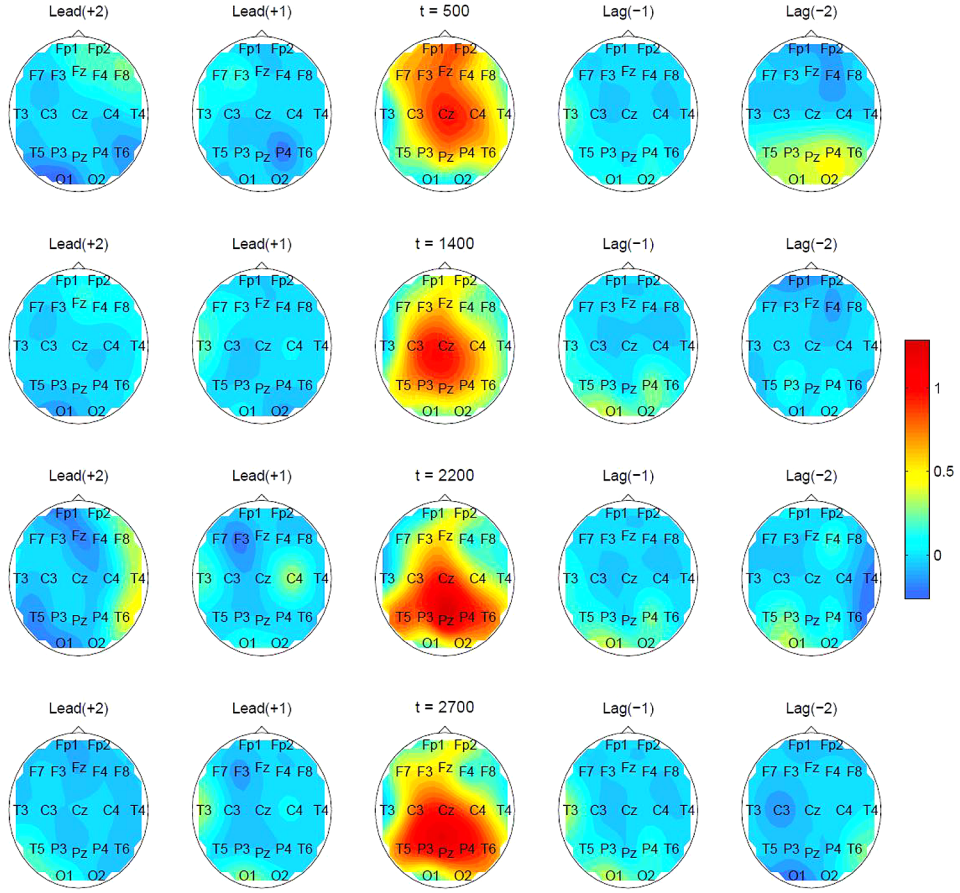
Figure 7 *EEG analysis: Estimated factor loadings $\hat{b}_{ikt}$ with the lag-lead structure at selected time points. The row-column layout of images corresponds to that in Figure* 6.

Animated figures provide more insights into the patterns of variation over time in factor loadings, the differences across channels, and the nature of the dynamic latent thresholding in particular. Such animations are available as on-line supplements to the paper[1]. A first animation[2] shows a movie of patterns of $\Pr(s_{ikt} = 1 | \boldsymbol{y}_{1:T})$ interpolating from values at the channels $i = 1:19$. This shows how these patterns evolve over time t, providing a dynamic display from which the snapshots in Figure 6 are selected at four specific times. A second animation[3] shows the corresponding movie for the interpolated estimates of factor loadings $\hat{b}_{ikt}$ over all time; the snapshots in Figure 7 are selected at four specific times. The

---

[1]Animation web page: www.stat.duke.edu/~mw/.downloads/NakajimaWest2016EEG/.

[2]Animation files animate-st.{avi,mp4}.

[3]Animation files animate-betat.{avi,mp4}.
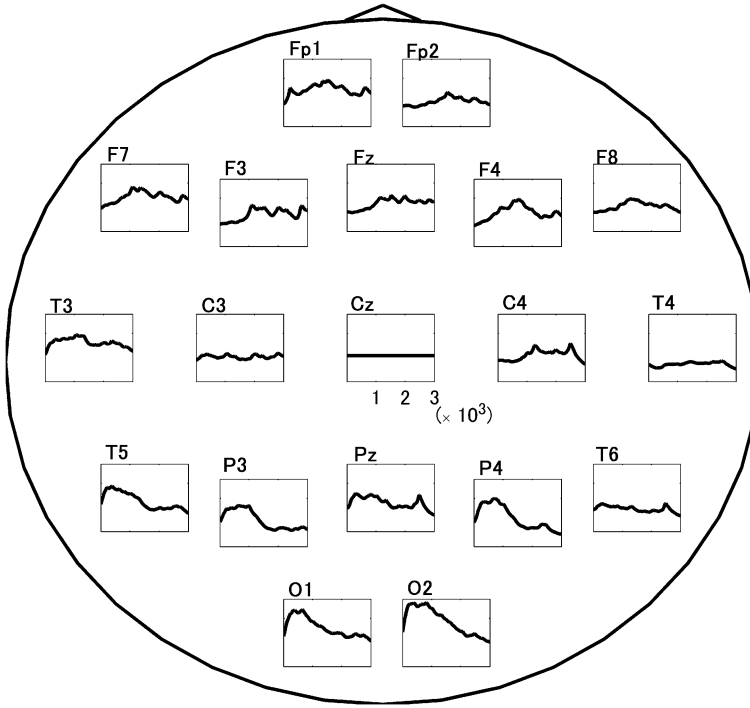
Figure 8 *EEG analysis: Trajectories of the posterior means of time-varying standard deviations of the idiosyncratic shocks, σ_{ikt}, across all channels $i = 1 : 19$. For clarity in presentation, the y-scale has been omitted; each standard deviation is graphed on the scale of 0–50 for comparability across channels. Recall that the anchor channel Cz has constant standard deviation representing pure measurement error around the latent process at that channel. Each graph is roughly located at the corresponding electrode placement and the x-axes represent the full time period $t = 1 : 3000$.*

animations clearly show and highlight regions of the brain surface where there is very low or negligible probability of lag or lead effects of the x_t process, other regions where sustained effects are very evident and regions in which there is more uncertainty about potential effects, together with inferences on the quantified lag/lead effects in terms of the temporal evolution of the spatial patterns in estimated factor loadings.

Figure 8 plots $E(\sigma_{ikt}|\mathbf{y}_{1:T})$, that is, estimated standard deviations of the idiosyncratic shocks in each channel $i = 1 : 19$. Each graph is roughly located at the corresponding electrode placement. Recall that $\sigma_{1t} = \sigma_1$, the innovation standard deviation for the channel Cz, is assumed time-invariant, representing measurement error only, as part of the model specification to define and identify the latent driving process x_t. The model allows for potential variations over time in standard deviations at other channels, with opportunity to identify variability in the data not already captured through the time-varying loadings and latent process structure.

From Figure 8, there do appear to be variations across channels and they show
some local spatial dependence. Trajectories of the neighboring channels F4 and
F8 are clearly similar, exhibiting a major hike in the middle of the seizure. It is
evident that some parietal and occipital sites (T3, P3, O1, O2 and P4) share a com-
mon trajectory, which marks a peak in an early stage of the seizure then gradually
decrease towards the end of the seizure. As seen in Figures 6 and 7, these sites
also share some relationships in the latent threshold-induced shrinkage and load-
ings at Lag(-1). Further, the estimate shows similarities among the channels Pz,
C4 and T6, whose patterns differ from those in the occipital region. This suggests
an intrinsic difference between the central sites (Pz, C4 and T6) and the occipital
sites (T3, P3, O1, O2 and P4), also suggested by Figures 6 and 7. Across all but
the vertex channel Cz at $i = 1$, the idiosyncratic error terms v_{it} represent a com-
pound of measurement error and of additional patterns including local sub-activity
of the seizure that is not explained by the latent factor process. There are also ex-
perimental and physiological noise sources that are likely to induce local/spatial
residual dependencies in the data not forming part of the main driving process
x_t, including electrical recording/power line noise and scalp-electrode impedance
characteristics; these presumably also contribute to the time-variation patterns in
the σ_{it} identified and their spatial dependencies.

5.4 Summaries from analysis of extended DTRFM Model M+

Model M+ has

$$\boldsymbol{y}_t = \boldsymbol{A}_t \boldsymbol{y}_{t-1} + \boldsymbol{B}_t \boldsymbol{f}_t + \boldsymbol{v}_t, \qquad \boldsymbol{v}_t \sim N(\boldsymbol{0}, \boldsymbol{\Sigma}_t), \tag{8}$$

where $\boldsymbol{A}_t$ is the $m \times m$ matrix of lag-1 time-varying coefficients modeled using
latent threshold AR(1) processes. Model M+ extends Model M to potentially
capture data structure not fully explained by the factor and residual component.
One interest is to more structurally explain the time variation in estimated resid-
ual volatilities σ_{it} exhibited in the analysis of the baseline Model M. A contex-
tual question is that of representing potential "spill-over" effects between EEG
channels as the seizure waves cascade around the brain; that is, local (in terms
of the neural network and perhaps in part, though not necessarily, physically spa-
tially) transmission of signals between subsets of channels that represent delayed
responses to the latent x_t process not already captured by the dynamic latent fac-
tor model form. The matrix $\boldsymbol{A}_t$ is expected to be sparse and modeled via latent
threshold dynamic models, as earlier described.

Figure 9 plots the posterior means of the states $\{\alpha_{ikt}\}$ and the posterior probabil-
ities $\Pr(s_{ikt}^a = 1 | \boldsymbol{y}_{1:T})$, where $s_{ikt}^a = I(|\alpha_{ikt}| \geq d_{ik}^a)$ and d_{ik}^a is the latent threshold
for each state α_{ikt}. The matrix $\boldsymbol{A}_t$ is evidently sparse and exhibits considerable
changes in the state and the posterior shrinkage probability among the selected
time points. Figure 10 shows the estimated standard deviations of the idiosyn-
cratic shocks $E(\sigma_{ikt} | \boldsymbol{y}_{1:T})$. Compared with Figure 8, the trajectories of standard
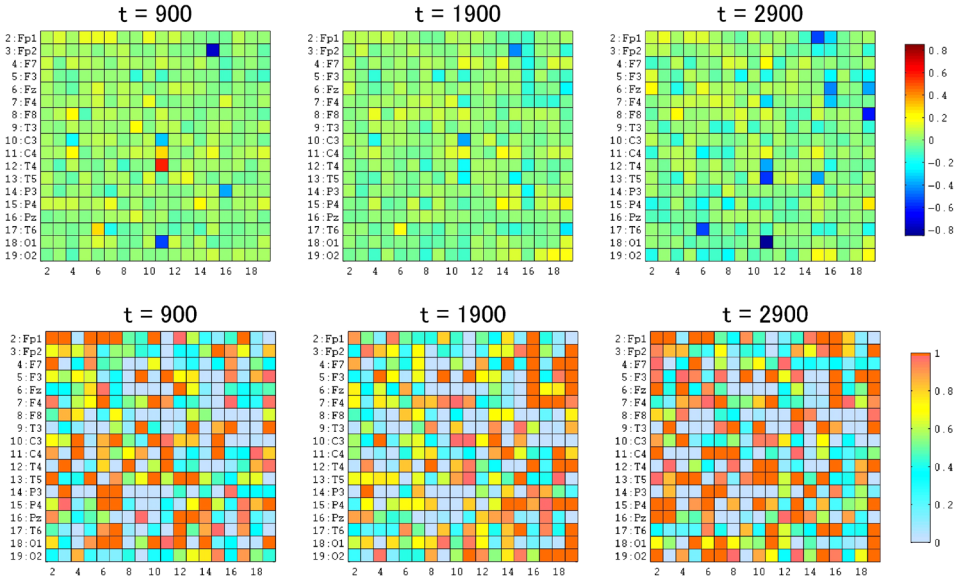
Figure 9 *EEG analyses*: *Posterior means of* $\{\alpha_{ikt}\}$ *(top) and posterior probabilities* $\Pr(s_{ikt}^a = 1 | \boldsymbol{y}_{1:T})$ *(bottom) for* $\boldsymbol{A}_t$, *in the TV-VAR extended model M+.*

deviations are generally somewhat smoother over time; some of the variation in the data not already captured by the $\boldsymbol{B}_t \boldsymbol{f}_t$ is now absorbed by the $\boldsymbol{A}_t \boldsymbol{y}_{t-1}$.

To explore some practical implications of the extended Model M+ and compare with the baseline Model M, one aspect of interest is predicted behavior of the time series based on *impulse response analysis* relative to the underlying x_t process. Standing at a current, specified time t, this simply asks about the nature of expected development of the series $\boldsymbol{y}_{t+1:t+h}$ over the next h time points based on an assumed level of the "impulse" $\epsilon_{t+1} = e$ to the driving innovations of the latent process. In applied work in economics, impulse responses are often primary vehicles for communicating model implications, comparing models, and feeding into decisions. The use of latent thresholding in macroeconomic models has focused on this, in part, and clearly demonstrated the utility of dynamic latent thresholding in inducing more accurate predictions and, in particular, more statistically and substantively reliable impulse response analyses (Nakajima and West (2013a)).

We do this here from three time points ($t = 900, 1900, 2900$) chosen in the early, middle and later sections of the EEG series; this exhibits differences in the model projections/implications over time due to the dynamics, as well as differences between the two models in each of these periods. Computations are easily done by using the posterior MCMC samples to project forward in time; predictive expectations are then computed as Monte Carlo averages. The impulse value e is taken as the average over $t = 1 : T$ of the estimated historical innovations standard deviations $E(w_t^{1/2} | \boldsymbol{y}_{1:T})$. Figure 11 plots the impulse responses of the 19 EEG
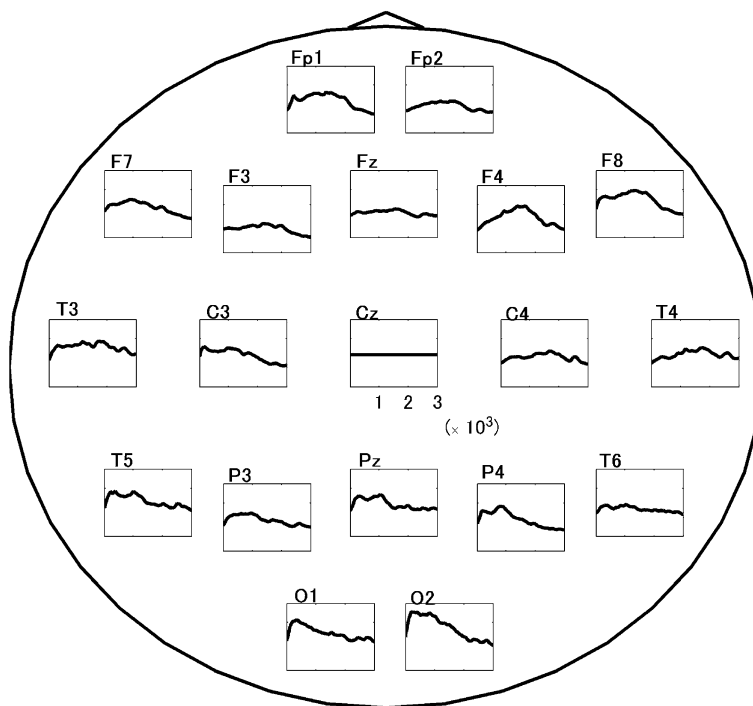
Figure 10 *EEG analysis*: *Trajectories of the posterior means of time-varying standard deviations of the idiosyncratic shocks*, σ_{ikt}, *across all channels* $i = 1 : 19$ *for the extended Model M+. Details as in as in Figure* 8 *for model M.*

channels with $h = 80$ and from each of the two models. Note that, for our comparison purposes here, we are interested in the *forms* of the impulse responses over the horizon specified, not their specific values. We already know that the innovations variance w_t shows marked changes over time and, in particular, decays to rather low values in the later stages of the seizure. Hence, the shock size e taken here is larger than relevant and realized innovations over the latter part of the time period, and the amplitudes of impulse responses should therefore not be regarded as pertinent. The form of the projections are the focus.
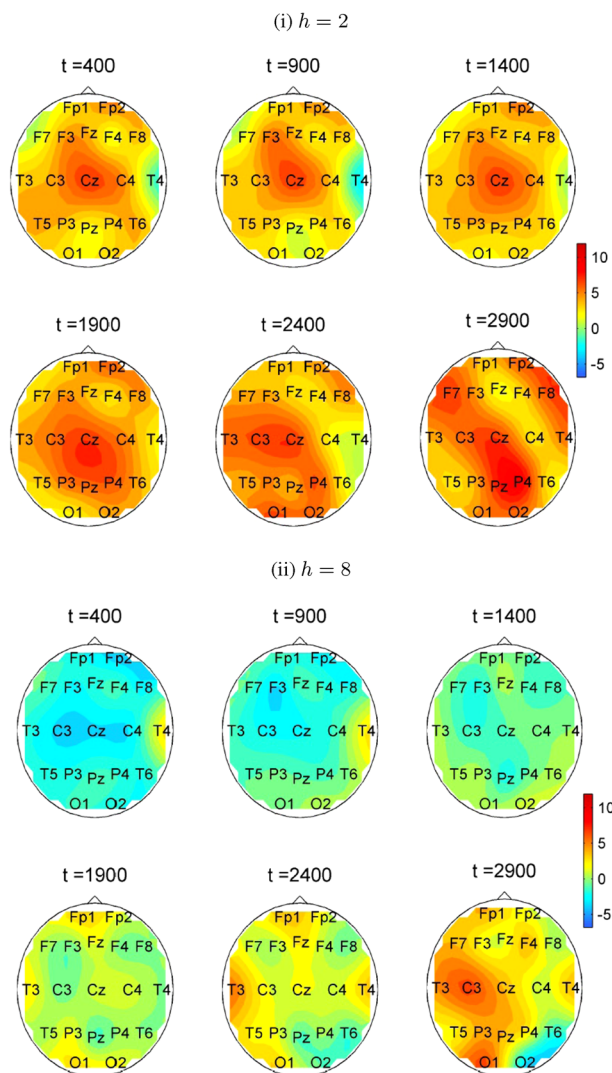
Patterns of the impulse response are clearly time-varying across the three exhibited time points; variation is evident with respect to wave frequency, persistence/decay speed, and variation across the channels. In early periods of the seizure, the responses decay slowly with a high-frequency cyclical wave, while in later periods the decay is more rapid and the oscillations at lower frequency. While there are, as we have discussed above, marked patterns of variation in lag/lead relationships across channels, there is the appearance of stronger synchronicity earlier in the seizure episode, and this deteriorates towards end of the seizure.

The responses from the TV-VAR extended Model M+ model exhibit more variation across the channels than those from the Model M. This is attributable to
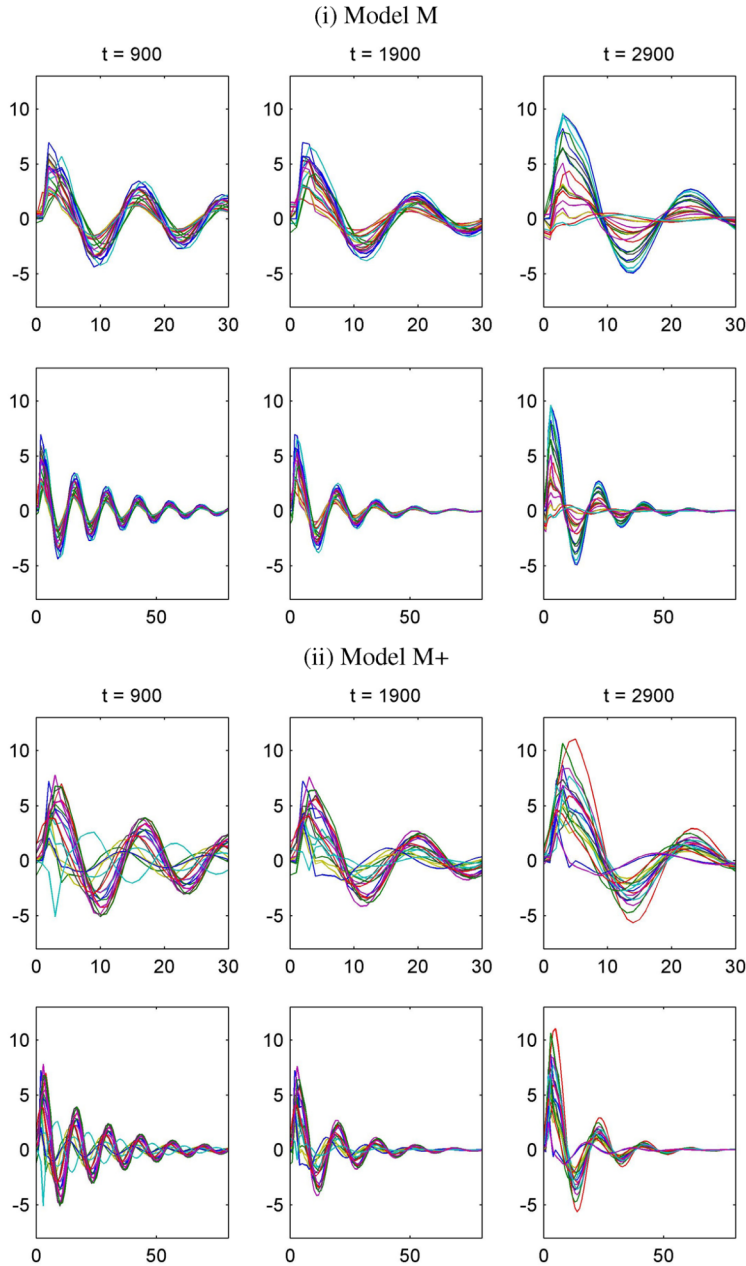
(i) Model M

(ii) Model M+

Figure 11 *EEG analyses: Impulse responses of the m = 19 EEG channels to a shock to the underlying factor process x_t obtained from (i) Model M, (ii) Model M+. The impulse response functions computed at three different time points throughout the seizure are shown (columns). For each model, the impulse response projections are made from the time point indicated by column header up to 80 time periods ahead (lower rows in (i) and (ii)); the same responses are shown on a truncated time period up to only 30 time periods ahead (upper rows in (i) and (ii)), for clarity.*

(i) $h = 2$

(ii) $h = 8$

Figure 12 *EEG analyses: Interpolated patterns of impulse responses from Model M+. These are computed at the six time points indicated, and shown for selected impulse response horizons $h = 2$ and 8, respectively.*

the induction of some spill-over effects of the shock. Through the latent factor model component alone, the shock $\epsilon_{t+1} = e$ has an impact on each of the channels through its immediate influence on x_{t+1} and the consequent transfer response of these effects via x_{t+1}, and so forth. In the extended model, additional feed-forward effects are passed through the channels via the TV-VAR component. Some additional insights into the nature of impulse responses can be gained from Figure 12 that shows images interpolating the 9 channel responses across the brain areas,

based on analysis of the extended Model M+. These are shown at six time points and for selected horizons $h = 2$ and 8, respectively; these images clearly show the time variation of the responses spreading over the channels.

An animated figure, available as an online supplement[4], provides a dynamic display over impulse response horizons 1:80, with a movie that more vividly exhibits the differences due to time period. The frames in the animation represent the six time points in Figure 12, and show images of the impulse responses as the projections are made over $t + 1, t + 2, \ldots, t + h$ to horizon $h = 80$.

6 Concluding remarks

The EEG time series analysis highlights the utility of latent thresholding dynamic models in constraining model parametrization adaptively in time, with resulting improvements in intepretation and inferences on inter-relationships among series and transfer response characteristics. An additional comment on model comparison in the case study is worth mentioning. Statistical evaluation and comparison of Model M+ with Model M is implicit since the latter is a special case of the former. The analysis results of M+ explicitly show the relevance of the extensions and hence support the more general model. This is separately supported by values of the deviance information criterion (DIC; see Spiegelhalter et al. (2002)) computed from the MCMC results for each model separately; this yields estimated DIC is 996,191.7 for Model M and 988,435.9 for Model M+, which indicates strong evidence that Model M+ dominates Model M.

A number of methodological and computational areas remain for further study. Among them, we note potential for integrating spatially-dependent structures with latent threshold factor models, motivated in part by the spatial-temporal findings in the EEG study. Also, incorporating two or more common latent processes might allow evaluation of more complex latent factor structures for these and other applications. Computational challenges are clear in connection with applying these models to higher dimensional time series such as are becoming increasing common in neuroscience as they are other other areas. That said, we expect the dynamic latent thresholding approach to become increasing relevant and important—in constraining and reducing effective parameter dimension via dynamic sparsity in model parameters—in contexts with higher-dimensional time series.

---

[4]Animation web page: www.stat.duke.edu/~mw/.downloads/NakajimaWest2016EEG/. Animation files animate-impulse.{avi,mp4}.

Appendix: Summary of MCMC analysis

Based on the observations $y_{1:T}$, the full set of latent state parameters and model parameters for the posterior analysis of DTRFM Model M is as follows:

- The latent factor process states $x_{-p+1:T}$ including uncertain initial values;
- The latent TVAR coefficient process $\delta_{1:T}$;
- The variance processes $\Sigma_{1:T}$ and $w_{1:T}$;
- The latent factor loading process $B_{0:T}$, including the uncertain initial state;
- The hyper-parameters $\theta = \{\mu_{ik}, \phi_{ik}, v_{ik}; i = 2 : m, k = 1 : r\}$ and Ψ;
- The latent threshold hyper-parameters $d_{2:m,1:r}$.

Key components of the MCMC are below. We simply note the states or parameters being generated, implicitly conditional on all other states and parameters.

Latent factor process states $x_{-p+1:T}$

The model of equations (1), (3) can be written in a conditionally linear, Gaussian dynamic model form with a modified state $\tilde{f}_t = (x_t, \ldots, x_{t-p+1})'$ and a state transition

$$\tilde{f}_t = G_t \tilde{f}_{t-1} + e_t, \tag{9}$$

where

$$G_t = \begin{pmatrix} \delta_{1t} & \delta_{2t} & \cdots & \delta_{p-1,t} & \delta_{pt} \\ 1 & 0 & \cdots & 0 & 0 \\ 0 & 1 & \cdots & 0 & 0 \\ \vdots & & \ddots & & \vdots \\ 0 & 0 & \cdots & 1 & 0 \end{pmatrix} \quad \text{and} \quad e_t = \begin{pmatrix} \varepsilon_t \\ 0 \\ 0 \\ \vdots \\ 0 \end{pmatrix}. \tag{10}$$

Generation of the full sets of states is obtained by the standard forward filtering, backward sampling (FFBS) algorithm (e.g., Prado and West (2010)), which is efficient in the sense that the full trajectories of the states over time are regenerated at each iterate of the overall MCMC.

TVAR coefficients

Conditional on $x_{-p+1:T}$ and the variances $w_{1:T}$, Ψ, equations (2), (3) reduce to a univariate, linear and Gaussian dynamic regression model with respect to the state process $\delta_{1:T}$. We sample the states using the FFBS algorithm.

TVAR innovations volatility

Based on the standard inverse gamma/beta Bayesian discount model for the variance sequence $w_{1:T}$ over time as noted in Section 3.2, the corresponding FFBS for volatilities provides a full sample from the conditional posterior for $w_{1:T}$ given all other quantities.

Observation variances

Similarly, the full conditional posterior for the $\mathbf{\Sigma}_{1:T}$ factorizes into m components involving the individual $\sigma_{i,1:T}$ separately over i, and the discount variance FFBS applies to each in parallel to generate full conditional posterior samples.

Factor loading process states

Following Nakajima and West (2013a, 2013b), we sample each $\boldsymbol{\beta}_t = \{\beta_{1:k,t}\}$ from its conditional posterior distribution given $\boldsymbol{\beta}_{-t} = \boldsymbol{\beta}_{0:T} \setminus \boldsymbol{\beta}_t$ and all other parameters. Recall that the elements of $\boldsymbol{\beta}_t$ follow standard AR(1) processes, but are linked to the observation equation by the latent threshold structure. The resulting conditional posterior for $\boldsymbol{\beta}_t$ is a non-standard distribution that we cannot directly sample. We use a Metropolis-within-Gibbs sampling strategy with the proposal distribution derived in the *non-threshold* case by assuming $s_{ikt} = 1$; that is, we generate the candidate from a standard linear dynamic model for $\boldsymbol{\beta}_t$ without the latent thresholds (see Section 2.3 of Nakajima and West (2013a)).

Hyper-parameters of AR and TVAR model components

Priors for the latent AR hyper-parameters $\boldsymbol{\theta}$ assume prior independence across series $i = 2:m$ with traditional forms: normal or log-gamma priors for μ_{ik}, truncated normal or shifted beta priors for ϕ_{ik}, and inverse gamma priors for v_{ik}^2. On this basis, the full conditional posterior for $\boldsymbol{\theta}$ breaks down into conditionally independent components across $i = 2:m$. We then resample the $(\mu_{ik}, \phi_{ik}, v_{ik}^2)$ in parallel across i, using direct sampling from the conditional posterior in cases that the priors are conditionally conjugate, or alternatively via Metropolis Hastings steps.

For the TVAR error variance matrix $\mathbf{\Psi}$, an inverse Wishart prior leads to an easily sampled inverse Wishart complete conditional posterior.

Latent thresholds hyper-parameters

As discussed in Section 3.2, the structured prior for the thresholds d_{ik} takes them as conditionally independent over $i = 2:m, k = 1:r$, with marginal priors that depend on the parameters of the corresponding latent AR processes, viz. $d_{ik} \sim U(0, |\mu_{ik}| + K u_{ik})$ where $u_{ik}^2 = v_{ik}^2/(1 - \phi_{ik}^2)$. The set of thresholds are then also independent in the complete conditional posterior; they are resampled in parallel via Metropolis Hastings independence chain steps using the conditional uniform priors as proposals. This is precisely as pioneered in Nakajima and West (2013a, 2013b) in other latent threshold models, and its efficacy has been borne out in a number of examples there.

Finally, note that the above requires a slight modification and extension to generalize the MCMC for the extended DTRFM Model M+ of Section 3.4. The extension now involves the TV-VAR parameter matrices $\mathbf{A}_{1:T}$ in equation (1) with $z_t = \boldsymbol{y}_{t-1}$, together with the required latent initial "missing" vector $\boldsymbol{y}_0$. The above
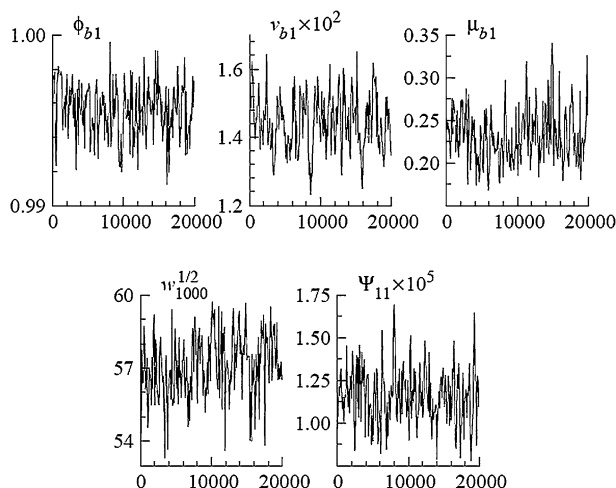
Figure 13   *EEG analyses*: *Typical MCMC trace plots for selected parameters.*

development applies conditional on these elements with the obvious modifications to subtract $A_t y_{t-1}$ from y_t throughout. Then additional MCMC steps are needed. First, y_0 is generated from a complete conditional normal posterior under a suitably diffuse normal prior. Second, the latent thresholded elements of the sequence $A_{1:T}$, and the set of hyper-parameters of the underlying AR(1) processes as well as the corresponding thresholds, are treated just as are the elements of $B_{1:T}$, discussed above. This component is a special case of the MCMC analysis for more general TV-VAR models as developed in Nakajima and West (2013a).

Comment on MCMC convergence

Some insights into the convergence of the MCMC sampling are gained by viewing trace plots for selected parameters. As an example, some such plots from the analysis of the extended Model M+ are shown in Figure 13.

About the authors

Jouchi Nakajima is Visiting Senior Economist in the Monetary and Economic Department of the Bank for International Settlements (BIS) in Basel, Switzerland, having earlier worked as Economist and Deputy Director of Global Economic Research at the Bank of Japan in Tokyo. His research interests include economic forecasting and policy, time series, econometric modeling and Bayesian computation, and applications in multiple areas. Nakajima holds BA and MA degrees in Economics from the University of Tokyo, as well as MS and PhD degrees in Statistical Science from Duke University.

Mike West is the Arts & Sciences Professor of Statistics and Decision Sciences in the Department of Statistical Science at Duke University. West works in theory and applications of Bayesian statistics broadly, with highlights in dynamic modeling, time series analysis and forecasting, and applications in many areas.

Acknowledgments

References

Aguilar, O., Prado, R., Huerta, G. and West, M. (1999). Bayesian inference on latent structure in time series (with discussion). In *Bayesian Statistics, Vol. 6* (J. M. Bernardo, J. O. Berger, A. P. Dawid and A. F. M. Smith, eds.) 3–26. Oxford: Oxford University Press. MR1723490

Aguilar, O. and West, M. (2000). Bayesian dynamic factor models and portfolio allocation. *Journal of Business and Economic Statistics* **18**, 338–357.

Bernanke, B., Boivin, J. and Eliasz, P. (2005). Measuring the effects of monetary policy: A factor-augmented vector autoregressive (FAVAR) approach. *The Quarterly Journal of Economics* **120**, 387–422.

Bhattacharya, A. and Dunson, D. B. (2011). Sparse Bayesian infinite factor models. *Biometrika* **98**, 291–306. MR2806429

Carvalho, C. M., Chang, J., Lucas, J. E., Nevins, J. R., Wang, Q. and West, M. (2008). High-dimensional sparse factor modeling: Applications in gene expression genomics. *Journal of the American Statistical Association* **103**, 1438–1456. MR2655722

Carvalho, C. M., Lopes, H. F. and Aguilar, O. (2011). Dynamic stock selection strategies: A structured factor model framework (with discussion). In *Bayesian Statistics, Vol. 9* (J. M. Bernardo, M. J. Bayarri, J. O. Berger, A. P. Dawid, D. Heckerman, A. F. M. Smith and M. West, eds.) 69–90. Oxford: Oxford University Press. MR3204454

Del Negro, M. and Otrok, C. M. (2008). Dynamic factor models with time-varying parameters: Measuring changes in international business cycles. Staff Report 326, Federal Reserve Bank of New York. DOI:10.2139/ssrn.1136163.

Doornik, J. A. (2006). *Ox: Object Oriented Matrix Programming*. London: Timberlake Consultants Press.

Dyro, F. M. (1989). *The EEG Handbook*. Boston: Little, Brown and Co.

Huerta, G. and West, M. (1999). Priors and component structures in autoregressive time series models. *Journal of the Royal Statistical Society, Series B* **61**, 881–899. MR1722245

Kimura, T. and Nakajima, J. (2016). Identifying conventional and unconventional monetary policy shocks: A latent threshold approach. *The BE Journals in Macroeconomics* **16**, 277–300.

Kitagawa, G. and Gersch, W. (1996). *Smoothness Priors Analysis of Time Series. Lecture Notes in Statistics* **116**. New York: Springer. MR1441074

Koop, G. and Korobilis, D. (2010). Bayesian multivariate time series methods for empirical macroeconomics. *Foundations and Trends in Econometrics* **3**, 267–358. DOI:10.1561/0800000013.

Koop, G. M. and Potter, S. (2004). Forecasting in dynamic factor models using Bayesian model averaging. *Econometrics Journal* **7**, 550–565. MR2103792

Lopes, H. F. and Carvalho, C. M. (2007). Factor stochastic volatility with time varying loadings and Markov switching regimes. *Journal of Statistical Planning and Inference* **137**, 3082–3091. MR2364152

Lopes, H. F. and West, M. (2004). Bayesian model assessment in factor analysis. *Statistica Sinica* **14**, 41–67. MR2036762

Lucas, J. E., Carvalho, C. M., Wang, Q., Bild, A. H., Nevins, J. R. and West, M. (2006). Sparse statistical modelling in gene expression genomics. In *Bayesian Inference for Gene Expression and Proteomics* (K. A. Do, P. Mueller and M. Vannucci, eds.) 155–176. Cambridge: Cambridge University Press. MR2269095

Lucas, J. E., Carvalho, C. M. and West, M. (2009). A Bayesian analysis strategy for cross-study translation of gene expression biomarkers. *Statistical Applications in Genetics and Molecular Biology* **8**, Article no. 11. MR2476389

Nakajima, J. and West, M. (2013a). Bayesian analysis of latent threshold dynamic models. *Journal of Business & Economic Statistics* **31**, 151–164. MR3055329

Nakajima, J. and West, M. (2013b). Bayesian dynamic factor models: Latent threshold approach. *Journal of Financial Econometrics* **11**, 116–153. DOI:10.1093/jjfinec/nbs013.

Nakajima, J. and West, M. (2015). Dynamic network signal processing using latent threshold models. *Digital Signal Processing* **47**, 6–15. MR3425313

Pitt, M. and Shephard, N. (1999). Time varying covariances: A factor stochastic volatility approach (with discussion). In *Bayesian Statistics, Vol. 6* (J. M. Bernardo, J. O. Berger, A. P. Dawid and A. F. M. Smith, eds.) 547–570. Oxford: Oxford University Press. MR1724873

Prado, R. (2010a). Characterization of latent structure in brain signals. In *Statistical Methods for Modeling Human Dynamics* (S. Chow, E. Ferrer and F. Hsieh, eds.) 123–153. New York: Routledge, Taylor and Francis.

Prado, R. (2010b). Multi-state models for mental fatigue. In *The Handbook of Applied Bayesian Analysis* (A. O'Hagan and M. West, eds.) 845–874. Oxford: Oxford University Press. MR2790366

Prado, R. and Huerta, G. (2002). Time-varying autoregressions with model order uncertainty. *Journal of Time Series Analysis* **23**, 599–618. MR1925266

Prado, R. and West, M. (2010). *Time Series Modeling, Computation, and Inference*. New York: Chapman & Hall/CRC.

Prado, R., West, M. and Krystal, A. D. (2001). Multichannel electroencephalographic analyses via dynamic regression models with time-varying lag-lead structure. *Journal of the Royal Statistical Society Series C Applied Statistics* **50**, 95–109.

Spiegelhalter, D. J., Best, N. G., Carlin, B. P. and van der Linde, A. (2002). Bayesian measures of model complexity and fit (with discussion). *Journal of the Royal Statistical Society, Series B* **64**, 583–639.

Weiner, R. D. and Krystal, A. D. (1994). The present use of electroconvulsive therapy. *Annual Review of Medicine* **45**, 273–281.

West, M. (1997). Time series decomposition. *Biometrika* **84**, 489–494.

West, M. (2003). Bayesian factor regression models in the "large p, small n" paradigm. In *Bayesian Statistics, Vol. 7* (J. M. Bernardo, M. J. Bayarri, J. O. Berger, A. P. David, D. Heckerman, A. F. M. Smith and M. West, eds.) 723–732. Oxford: Oxford University Press. MR2003537

West, M. (2013). Bayesian dynamic modelling. In *Bayesian Theory and Applications, Vol. 8* (P. Damien, P. Dellaportes, N. G. Polson and D. A. Stephens, eds.) 145–166. Oxford: Oxford University Press. MR3221162

West, M. and Harrison, P. J. (1997). *Bayesian Forecasting and Dynamic Models*, 2nd ed. New York: Springer. MR1482232

West, M., Prado, R. and Krystal, A. D. (1999). Evaluation and comparison of EEG traces: Latent structure in nonstationary time series. *Journal of the American Statistical Association* **94**, 375–387.

Yoshida, R. and West, M. (2010). Bayesian learning in sparse graphical factor models via annealed entropy. *Journal of Machine Learning Research* **11**, 1771–1798. MR2653356

Zhou, X., Nakajima, J. and West, M. (2014). Bayesian forecasting and portfolio decisions using dynamic dependent factor models. *International Journal of Forecasting* **30**, 963–980. DOI:10.1016/j.ijforecast.2014.03.017.

Monetary and Economic Department
Bank for International Settlements (BIS)
Centralbahnplatz 2
4051 Basel
Switzerland
E-mail: jouchi.nakajima@bis.org

Department of Statistical Science
Duke University
Durham, North Carolina 27708-0251
USA
E-mail: Mike.West@duke.edu